Published in final edited form as:
Neuroimage. 2012 February 15; 59(4): 3563–3570. doi:10.1016/j.neuroimage.2011.11.046.

Individualized localization and cortical surface-based registration of intracranial electrodes

Andrew R. Dykstra[1,3,*], **Alexander M. Chan**[2,3,*], **Brian T. Quinn**[4], **Rodrigo Zepeda**[3], **Corey J. Keller**[3], **Justine Cormier**[3], **Joseph R. Madsen**[5], **Emad N. Eskandar**[6], and **Sydney S. Cash**[3]

[1]Harvard-MIT Division of Health Sciences and Technology, Program in Speech and Hearing Bioscience and Technology, Cambridge, MA

[2]Harvard-MIT Division of Health Sciences and Technology, Program in Medical Engineering and Medical Physics, Cambridge, MA

[3]Cortical Physiology Laboratory, Department of Neurology, Massachusetts General Hospital and Harvard Medical School, Boston, MA

[4]Comprehensive Epilepsy Center, New York University School of Medicine, New York, NY

[5]Department of Neurosurgery, Brigham and Women's Hospital and Harvard Medical School, Boston, MA

[6]Department of Neurosurgery, Massachusetts General Hospital and Harvard Medical School, Boston, MA

Abstract

In addition to its widespread clinical use, the intracranial electroencephalogram (iEEG) is increasingly being employed as a tool to map the neural correlates of normal cognitive function as well as for developing neuroprosthetics. Despite recent advances, and unlike other established brain mapping modalities (e.g. functional MRI, magneto- and electroencephalography), registering the iEEG with respect to neuroanatomy in individuals – and coregistering functional results across subjects – remains a significant challenge. Here we describe a method which coregisters high-resolution preoperative MRI with postoperative computerized tomography (CT) for the purpose of individualized functional mapping of both normal and pathological (e.g., interictal discharges and seizures) brain activity. Our method accurately (within 3mm, on average) localizes electrodes with respect to an individual's neuroanatomy. Furthermore, we outline a principled procedure for either volumetric or surface-based group analyses. We demonstrate our method in five patients with medically-intractable epilepsy undergoing invasive monitoring of the seizure focus prior to its surgical removal. The straight-forward application of this procedure to all types of intracranial electrodes, robustness to deformations in both skull and brain, and the ability to compare electrode locations across groups of patients makes this procedure an important tool for basic scientists as well as clinicians.

Corresponding author: Andrew R. Dykstra, Address: Thier 423, 45 Fruit St. Boston, MA 02114, Telephone: 617.895.7195, adykstra@mit.edu.

*These authors contributed equally to this work.

Keywords

electrocorticography; image registration; epilepsy; ct; mri

1. Introduction

In a large subset of patients with complex partial epilepsy, pharmacological intervention is ineffective (Engel et al. 2005). If non-invasive measures (e.g. EEG, PET, fMRI) fail to sufficiently localize the epileptogenic zone or if that zone abuts or overlaps eloquent cortex, arrays of electrodes placed either directly on the cortical surface or into deep structures (e.g. hippocampus, amygdala) may be indicated. Since its inception (Penfield & Jasper 1954; Engel et al. 2005), iEEG has been the gold-standard method for localizing seizure foci and delineating eloquent cortex in patients with medically-intractable epilepsy. Owing to its high spatiotemporal resolution and simultaneous coverage of wide areas of cortex, iEEG is increasingly being used as a tool to study the neural correlates of normal cognitive function (e.g., Crone et al. 2001; Yoshor et al. 2007; Brugge et al. 2008; Jerbi et al. 2009; Sahin et al., 2009) and examine spontaneous brain activity (e.g., Canolty et al. 2006; He et al. 2008; Cash et al. 2009). It has proven particularly informative in studying certain aspects of brain activity (e.g. gamma-band activity) which are less observable with non-invasive methods (i.e., EEG or MEG). More recently, intracranial electrodes are also being used as a recording platform from which to design brain-computer interfaces for various neuroprosthetic purposes, including communication aids for patients who suffer from amyotrophic lateral sclerosis or stroke (e.g., Wilson et al. 2006; Leuthardt et al. 2006; Felton et al. 2007; Schalk et al. 2008; Schalk 2010; Shenoy et al. 2008).

For clinical as well as scientific purposes – including seizure-onset localization, eloquent-cortex mapping, and cross-subject comparison, as well as relating results to other neuroanatomical structures (e.g. white matter tracts) and the larger neuroimaging literature knowledge of electrode location with respect to the patient's individual neuroanatomy is critical. This is especially true given the spatial specificity of iEEG (due to its proximity to neural generators). Despite its importance, registering iEEG with a patient's individual cortical folding pattern remains a major challenge. Several solutions to this problem have been proposed, utilizing photography (Wellmer et al. 2002; Mahvash et al. 2007; Dalal et al. 2008), 2D radiography (Miller et al. 2007), postoperative MRI (Bootsveld et al. 1994; Kovalev et al. 2005; Hugh Wang et al., Comprehensive Epilepsy Center, New York University School of Medicine, personal communication), or postoperative CT (Grzeszczuk et al. 1992; Winkler et al. 2000; Noordmans et al. 2001; Nelles et al. 2004; Hunter et al. 2005; Tao et al. 2009; Hermes et al. 2010), each with inherent limitations.

Here, we describe an electrode-localization procedure which combines the coregistration of high-resolution preoperative MRI with postoperative CT and the 3D rendering of each patient's cortical surface (Dale et al. 1999; Fischl et al. 1999a) or volumetric reslicing to align the slice with the long axis of depth-electrode arrays. The parenchymal shift introduced by the implantation of subdural electrodes (Hill et al. 1998; Hill et al. 2000; Hastreiter et al. 2004; Miyagi et al. 2007; Dalal et al. 2008; Hermes et al. 2010), which can often be larger than a centimeter (Hill et al. 1998), potentially causing localization errors at least this large (Dalal et al. 2008), is accounted for by using an optimization algorithm that minimizes an energy function defined by inter-electrode distances and global deformation of electrode configuration. This method minimizes assumptions about the nature of the parenchymal shift introduced by the implant and allows for accurate localization of electrodes near highly convex cortical regions. We extend previous work by providing a procedure for cortical surface-based intersubject registration of each individual's electrode

ensemble, allowing for surface-based group analyses of studies utilizing subdural electrodes. Given the fact that subdural electrodes are positioned on the cortical surface, this method of group analysis should prove more accurate when compared to the standard volumetric-based analyses (Collins et al. 1994; Miller et al. 2007; Ritzl et al. 2007; Talairach & Tournoux 1988). We validate our registration method by comparison with intraoperative photographs, using prominent anatomical landmarks in order to determine the distance between estimated and actual electrode locations in reference to the 3D cortical reconstruction.

2. Materials and Methods

2.1. Patients

Five patients with medically-intractable epilepsy underwent clinically-indicated invasive monitoring of the seizure focus prior to its surgical removal (Table 1). Patients gave their informed consent, and all procedures were approved by the Institutional Review Boards at Partners Healthcare (Massachusetts General Hospital and Brigham and Women's Hospital) and the Massachusetts Institute of Technology. Prior to electrode implantation, each patient underwent high-resolution T1-weighted MRI. No corrections for potential B-field distortions were applied. During the implantation procedure, patients were placed under general anesthesia, a craniotomy was performed, and the overlying dura was reflected over the intact skull to expose the lateral aspect of the cortical surface (Fig. 1A and Fig. 1B). In each patient, arrays of platinum electrodes embedded in silastic sheets (2.3mm exposed diameter, 10mm center-to-center spacing, *Adtech Medical, Racine, WI*) were placed over temporal, frontal, and parietal cortex. In some cases inferior temporal, interhemispheric, and occipital cortex was covered as well. The reflected dura was then sewn over the electrode array and the skull was replaced. After a brief recovery period, each patient underwent postoperative CT in order to assess electrode placement and to verify the absence of hemorrhage and mass effect.

2.2. Coregistration of preoperative MRI with postoperative CT

High-resolution postoperative CT was automatically registered to the same patient's preoperative MRI using the mutual-information-based transform algorithm provided by SPM (http://www.fil.ion.ucl.ac.uk/spm/; Wells et al. 1996) in the Freesurfer environment (http://surfer.nmr.mgh.harvard.edu/fswiki/FreeSurferWiki). Using the CT scan as the movable volume, the registration was visually checked and, if necessary, manually adjusted. Fig. 1D shows an example of this registration for a single patient.

2.3. Manual selection of electrode coordinates

Electrode coordinates were obtained in the patient's native anatomical space by visual inspection in the Freesurfer environment using *tkmedit*. Nearly all electrodes from an individual patient can be visualized in a 2D image by computing the maximum intensity projection of the CT volume in the plane approximately perpendicular to the long axis of the electrode arrays (usually sagittal for subdural arrays as shown in Fig. 1C and Figure 3a, and usually coronal or horizontal for stereotactically-placed depth arrays). Doing so significantly reduces the time it takes to manually localize each electrode in three dimensions and transcribe its coordinate (either native Freesurfer RAS or MNI space). After locating each electrode in the 2D image, the final electrode coordinates were obtained by traversing slices in the 3rd dimension (through the plane in Fig. 1C) and selecting the approximate center of the hyper intensity created by each electrode. Each electrode's coordinate (in native RAS space) was then manually transcribed. This procedure yielded an initial estimate of a subdural electrode's coordinate on the cortical surface or a depth electrode's position within the volume.

2.4. Volumetric reslicing for visualization of depth-electrode arrays

In order to visualize all electrodes from a signal depth array, new slices from the 3D MRI volume were computed which aligned the new slices with long axis of each array. In general, stereotactic depth arrays are placed orthogonal or near-orthogonal to the sagittal plane; thus, reslicing was performed to yield peri-coronal or peri-horizontal images. The peri-coronal or peri-horizontal plane for each new slice was defined by the most-superfical and deepest contacts. A simple linear equation is used to determine the reslicing plane, and a weighted average of the intensities adjacent voxels is used to generate the final slice image. The following equations were used to determine a peri-coronal slice.

$$m=\frac{e_{1y}-e_{ny}}{e_{1x}-e_{nx}}$$

$$b=e_{1y}-me_{1x}$$

$$y=mx+b$$

$$I_s(x,z)=\text{frac}(y)*I_v(x,\text{floor}(y),z)+[1-\text{frac}(y)]*I_v(x,\text{ceil}(y),z)$$

In these equations, the slope, m, and intercept, b, are computed using the most medial, e_1, and most lateral electrodes, e_n, where x is the right-left axis, y is the anterior posterior axis, and z is the superior-inferior axis. The pixel intensities of the final slice, I_s, are computed as the weighted average of adjacent voxel intensities, Iv, along the new slice plane. Results using such volumetric reslicing are shown in Fig. 2.

2.5. Construction of pial and dural surfaces

3D rendering of each patient's cortical surface was performed in the Freesurfer environment using high-resolution T1-weighted MRI. No corrections were made for potential B-field distortions. Talairach registrations (using the Freesurfer talairach volume as a movable template) and white and gray matter surfaces were inspected and manually corrected if necessary. After a satisfactory pial surface was obtained, a smoothed pial surface (effectively a dural surface, Fig. 3b) was computed for both hemispheres using the morphological closing algorithm built into Freesurfer (Schaer et al. 2008).

2.6. "Snapping" surface electrode coordinates to the cortical surface

Due to brain deformation known to be caused by the implant procedure (Hill et al. 1998), initial electrode coordinates obtained from CT scans (coregistered with preoperative MRI) appear buried within the parenchyma instead of on the cortical surface when overlaid onto the cortical reconstruction (left panels of Fig. 3b). Our method accounts for this deformation automatically in two steps: (1) pulling the initial coordinate estimates to the dural surface via an energy minimization algorithm and (2) projecting the coordinates from the dural surface to the closest vertex on the pial surface (lower right panel of Fig. 3b).

The electrode coordinates are initially pulled to the dural surface using a constrained energy minimization algorithm. The algorithm must fulfill the constraint that all electrodes lie on

the dural surface, while minimizing the displacement between the original and current electrode locations, as well as the deformation in the spatial configuration of the electrodes. The energy function is therefore composed of a displacement term as well as a deformation term and is defined as,

$$E(e)=E_{displacement}+E_{deformation}=\sum_{i=1}^{N}\left\|e_i-e_i^0\right\|^2+\sum_{i=1}^{N}\sum_{j=i+1}^{N}\alpha_{ij}\left(d_{ij}-d_{ij}^0\right)^2$$

with the constraint,

$$\forall i,\left\|e_i-s_i\right\|=0$$

where N is the number of electrodes, e_i is the location of electrode i, e_i^0 are the original coordinates for electrode i, d_{ij} is the distance between electrodes i and j, d_{ij}^0 is the original distance between that same pair of electrodes, α_{ij} is a parameter which takes values 1 or 0 determining whether the pair of electrodes i and j contribute to the energy function, and s_i is the location on the dural surface closest to electrode i.

Intuitively, the energy algorithm places a series of “springs” between each electrode and its original position (displacement springs), as well as springs between the electrodes themselves (deformation springs). The energy in each spring increases if the electrodes are pulled apart or pushed together further than their equilibrium distance (0 for displacement springs, α_{ij} for deformation springs).

Ideally, the pairs of electrodes which define adjacent contacts on a grid or strip of electrodes would be included in the deformation term of the energy function (α_{ij}= 1), while distant pairs of electrodes would not exert an influence on the energy minimization (α_{ij}= 0). This would result in a mesh-like structure of springs which prevents individual electrodes from greatly deviating from the initial spatial configuration, but allows for “bending” or “flexing” of the silastic grids and strips (Fig. 4a). To automatically determine the pairs of electrodes included in the energy function, the 5 nearest neighbors for each electrode are computed, and placed into quantized bins with 0.2mm resolution. After this is completed for all electrodes within a given patient, the bin with the largest count is taken as the “fundamental” distance between contacts. Hypothetical springs are placed between any two electrodes i and j falling within 1.25x of the fundamental distance (i.e. α_{ij} is set to 1 for the pair of electrodes i and j). At most, each electrode may have 5 connections. Any electrode which still does not have any connections is connected to its nearest neighbor as well as any other contact lying with 1.25x the distance to its nearest neighbor. This guarantees that all electrodes have at least one connection, and allows for strips that may have electrode spacings larger than the fundamental distance. Note that this algorithm also takes into account the possibility of multiple arrays with different electrode spacings.

The optimization was performed in MATLAB using the *fmincon* algorithm in the optimization toolbox. The optimization was set to terminate when the total constraint function was less than 0.01*N, the change in the energy function was less than 0.03, or the change in e was less than 0.1. The total number of iterations was limited to 50.

After the electrodes are pulled to the dural surface, they are projected to the closest vertex (in Euclidean distance) on the pial surface. This second projection is necessary for functional mapping within an individual as well as accurate projection to the Freesurfer average brain (see section 2.8).

2.7. Validation

Validation of our localization procedure was carried out in two of five patients through visual inspection of intraoperative photographs and comparison with estimated electrode locations in reference to the reconstructed cortical surface. For electrodes which were visible in intraoperative photographs, local anatomical landmarks including prominent sulci and gyri were used to estimate, manually, an electrode's actual position on the reconstructed surface. Subsequently, for each electrode, the Euclidean distance between the location estimated by the MR-CT procedure and that determined by visual inspection of the photographs was computed. We used this distance as a measure of error.

2.8. Surface-based coregistration with Freesurfer average brain

For each patient, we computed a 2D spherical rendering of the pial surface and coregistered it with the average spherical surface provided in Freesurfer. Electrode (excluding depth electrodes) coordinates from an individual were then transformed to the individual's registered spherical surface using a one-to-one look-up table, projected onto the spherical Freesurfer average surface by nearest-neighbor transformation. Finally, these coordinates were overlaid onto the template pial surface by one-to-one look-up table (Fig. 3d). Given that this registration method is known to yield better alignment of structural as well as functional brain areas across subjects (Fischl et al. 1999b) and the fact that subdural electrodes most often rest on or near gyral crowns, projecting electrode coordinates from an individual's pial surface onto a template brain by spherical means could prove useful for group studies.

3. Results

3.1. Individual localization

Fig. 3B shows the results of our projection method for an individual subject implanted with four 2×8 and one 1×8 strip arrays. As can be seen in the upper and lower left-hand panels of Fig. 3B, several electrodes are either invisible or outside the brain as defined by the smoothed pial surface. After the snapping procedure outlined in section 2.5 was performed (Fig. 4), the electrodes now appear on the smoothed pial surface (upper right-hand panel of Fig. 3B), and were finally snapped to the original pial surface by nearest-neighbor mapping (lower right-hand panel of Fig. 3B).

3.2. Cross-subject registration

Unlike more established brain-mapping modalities such as fMRI, the ability to cross-register functional intracranial recordings across various individuals has proven difficult. The accurate localization of electrodes within individuals could allow for cognitive generalizations if those locations could be compared across subjects.

Fig. 3C and Fig. 3D show the surface-based coregistration of a single subject with the Freesurfer average surface (Fischl et al., 1999b). The 2D spherical surface of the individual subject is shown in the lower panel of Fig. 3C (Fischl et al., 1999a). Gyri and sulci are indicated by green and red, respectively. This surface has been coregistered with the Freesurfer average surface, shown in the upper panel of Fig. 3C using the procedure described in Fischl et al., 1999b. Each electrode coordinate was projected from the individual's pial surface (lower-right panel of Fig. 3B) to the same individual's spherical

surface by a one-to-one mapping of the vertex. Electrode coordinates were then projected onto the Freesurfer average brain by nearest-neighbor mapping defined by Euclidean distance in the 2D spherical space. Electrodes from an individual subject after having been projected onto the Freesurfer average are shown in Fig. 3D. Fig. 5 shows the results of the spherical registration procedure collapsed across all five subjects in the study after each subject's cortical surface was aligned with that of the Freesurfer average. While electrodes from different patients rarely overlap, this mapping allows direct comparison across subjects.

Note that this procedure does not apply to electrodes on penetrating depth arrays.

3.3. Validation

Estimates of the error in the electrode localization procedure were obtained in 2 of the 5 subjects in the study by manual inspection of electrodes visible in intraoperative photographs (Fig. 1A and Fig. 1B). An electrode's true location on the cortical surface was estimated with reference to major anatomical landmarks (e.g. gyri/sulci and/or vascular features). The estimated difference between the true electrode locations and those obtained by our localization procedure was 2.52mm and 3.00mm in patient 3 and patient 5, respectively. Interquartile ranges as well as minimum and maximum errors are given in table 2.

3.4. Brain deformation due to implant

Assuming the level of accuracy established by our validation, our method allows for the quantitative measurement of the amount of deformation of the parenchyma due to the implantation of chronic sub-dural electrodes by quantifying the distance between initial estimates of an electrode's location and that after our automated "snapping" procedure. Fig. 6 shows the distributions of electrode displacements for each of the five patients in our study, as well as the collated distribution from all five patients. The median displacement of the pial surface across all five patients was 3.04mm, but displacements could be as large as 1.38cm.

3.5. Example of method's utility

To illustrate application of the localization method, Fig. 7 shows the spatiotemporal voltage pattern of a single interictal discharge in patient 5 from 100 ms before to 1000 ms after the peak of the discharge. As can be seen from this figure, the discharge initiates at around 70ms along the superior aspect of the inferior frontal gyrus and subsequently spreads dorsally and ventrally to include the posterior middle frontal gyrus, anterior inferior frontal gyrus, and possibly anteroventral temporal areas. The initial spike was followed by a broader slow wave that initiated at approximately 200ms and continued throughout the remainder of the times shown in the figure. Note that in this case, a relatively small error in electrode localization would lead to mislocalization of the source of the interictal discharge, possibly placing it in the middle vs. inferior frontal gyrus and possibly leading to a resection of the wrong tissue by the neurosurgeon. The same concerns of anatomical precision extends to studies of normal cognitive function, albeit with lesser clinical consequence for the implanted individual. Our method has recently been used to compare low-frequency (< 0.1 Hz) resting-state fMRI networks with corticocortical evoked potentials elicited by single-pulse stimulation with intracranial EEG electrodes (Keller et al. 2011). Without the localization accuracy our method provides, functional-anatomical correlations between BOLD activity and iEEG could not have been established.

4. Discussion

The localization of intracranial electrodes is a critical issue in electrocorticography for clinical as well as scientific purposes. We have demonstrated a method for accurately aligning a postoperative CT scan with preoperative MRI for the purpose of individualized localization of semichronic intracranial electrodes. The method coregisters preoperative MRI with postoperative CT using a combination of an automatic mutual information-based procedure (Wells et al., 1996) and visual inspection. After this alignment, electrode coordinates were obtained manually using Freesurfer and projected onto the pial surface using a combination of an energy-minimization function and nearest-neighbor mapping. Our method affords patient-specific localization accuracy with estimated error on the order of half a centimeter or less, comparable with previously-demonstrated methods using either a similar CT-MRI method (Hermes et al., 2010) or a method utilizing X-rays and intraoperative photographs (Dalal et al., 2008).

The main advantages of our method include (i) the same initial coregistration procedure operates on either subdural electrodes or depth electrodes accessing the mesial temporal-lobe structures (Fig. 2), (ii) it minimizes assumptions about the parenchymal shift (Hill et al. 1998; Hill et al. 2000; Hastreiter et al. 2004; Miyagi et al. 2007; Dalal et al. 2008; Hermes et al. 2010) introduced by the implant by using an optimization procedure to project the electrodes to the smoothed pial surface, (iii) it provides a procedure for cortical-surface-based intersubject mapping (Fig. 5), (iv) – as mentioned by others (Hermes et al., 2010) – it can accurately localize electrodes positioned anywhere in the volume, rather than solely those in the vicinity of the craniotomy or away from highly convex areas such as the ventral temporal lobes, and (v) the method relies on very little commercial software (with the exception being MATLAB). With respect to (ii), our method provides a particular advantage over local-norm-based projection (Hermes et al., 2010) in that it applies equally well to different electrode configurations (e.g., 8×8 vs. 1×8) because it does not rely on the computation of a normal vector for which there may be no unique solution, e.g. in the case of 1xN array.

Our method is useful for basic scientific as well as clinical purposes. Knowledge of electrode location is critical for the interpretation of cognitive experiments and allows clinicians to extraoperatively visualize ictal and interictal activity at anatomically correct locations, possibly mitigating risk to the patient by reducing the need for intraoperative mapping. The surface-based intersubject mapping procedure is especially useful for group studies. It has been shown previously that 2D spherical alignment of individual brains provides far greater localization accuracy of both structural and functional neuroanatomical features when compared with volumetric-based alignment methods (Fischl et al., 1999b). This is especially likely to be the case for subdural electrode studies given that each electrode rests on or near the crown of a gyrus. A surface-based procedure is also likely to yield better overlap between electrocorticography findings and those from non-invasive methods such as functional MRI, scalp EEG, and magnetoencephalography.

Both the MRI-CT coregistration and the pial-surface projection are likely to introduce some localization error. The pial-surface projection error occurs due to some electrodes positioning between adjacent gyri over the intervening sulcus. However, in order to perform intersubject surface-based registration, the error introduced by the pial-surface projection is unavoidable; thus, most of the correctable error is likely due to subtle inaccuracies in the MRI-CT registration. In our method, this registration was semi-automated, using a mutual-information-based algorithm shown previously to provide good alignment of within-subject multimodal images (Wells et al., 1996). This procedure is rendered more difficult, however, by the deformation of the skull caused by the craniotomy, and manual adjustments were

often required. In our experience, scans yielding high-resolution isotropic or near-isotropic voxels provided the best initial coregistration estimate with the preoperative MR volume. In principle, it should be possible to use only the hemisphere opposite the craniotomy in computing the MRI-CT registration. This is likely to yield better automatic registration estimates but would require manual editing of the CT volume in order to mask the hemisphere with the craniotomy-induced deformations.

One limitation of our method is the time it takes to manually localize each electrode in the coregistered CT volume. Automation of the electrode localization would significantly reduce the time spent during this step. A possible automation algorithm would use the dural surface as an inclusive volumetric mask for the CT volume after the MRI and CT have been coregistered. This would prevent the extraneous metal (e.g. wires and connectors) often included within the CT's field of view from generating false alarms during automatic electrode detection. A similar procedure has previously been described for coregistering preoperative and postoperative MR images (Kovalev et al., 2005). However, such an automation procedure would only be useful as a first pass electrode localization, and manual validation would likely still be required.

Acknowledgments

The authors thank the patients and their families for their participation, Naoro Tanaka and Steve Stufflebeam for providing cortical reconstructions for patients 4 and 5, neurology staff at both Massachusetts General Hospital and Brigham and Women's Hospital for assistance in data collection as well as Eric Halgren and Thomas Thesen for helpful comments.

References

Bootsveld, K., et al. [Accessed September 27, 2010] Localisation of intracranial EEG electrodes using three dimensional surface reconstructions of the brain. European Radiology. 1994. Available at: http://www.springerlink.com/content/wq4t753481u36412/

Brugge JF, et al. Functional localization of auditory cortical fields of human: click-train stimulation. Hearing Research. 2008; 238(1–2):12–24. [PubMed: 18207680]

Canolty RT, et al. High gamma power is phase-locked to theta oscillations in human neocortex. Science (New York, NY). 2006; 313(5793):1626–1628.

Cash SS, et al. The human K-complex represents an isolated cortical down-state. Science (New York, NY). 2009; 324(5930):1084–1087.

Collins DL, et al. Automatic 3D intersubject registration of MR volumetric data in standardized Talairach space. Journal of Computer Assisted Tomography. 1994; 18(2):192–205. [PubMed: 8126267]

Crone NE, et al. Induced electrocorticographic gamma activity during auditory perception. Brazier Award-winning article, 2001. Clinical Neurophysiology: Official Journal of the International Federation of Clinical Neurophysiology. 2001; 112(4):565–582. [PubMed: 11275528]

Dalal SS, et al. Localization of neurosurgically implanted electrodes via photograph-MRI-radiograph coregistration. Journal of Neuroscience Methods. 2008; 174(1):106–115. [PubMed: 18657573]

Dale AM, Fischl B, Sereno MI. Cortical surface-based analysis. I. Segmentation and surface reconstruction. NeuroImage. 1999; 9(2):179–194. [PubMed: 9931268]

Engel AK, et al. Invasive recordings from the human brain: clinical insights and beyond. Nature Reviews Neuroscience. 2005; 6(1):35–47.

Felton EA, et al. Electrocorticographically controlled brain-computer interfaces using motor and sensory imagery in patients with temporary subdural electrode implants. Report of four cases. Journal of Neurosurgery. 2007; 106(3):495–500. [PubMed: 17367076]

Fischl B, Sereno MI, Dale AM. Cortical surface-based analysis. II: Inflation, flattening, and a surface-based coordinate system. NeuroImage. 1999a; 9(2):195–207. [PubMed: 9931269]

Fischl B, Sereno MI, Tootell RB, et al. High-resolution intersubject averaging and a coordinate system for the cortical surface. Human Brain Mapping. 1999b; 8(4):272–284. [PubMed: 10619420]

Grzeszczuk R, et al. Retrospective fusion of radiographic and MR data for localization of subdural electrodes. Journal of Computer Assisted Tomography. 1992; 16(5):764–773. [PubMed: 1522271]

Hastreiter P, et al. Strategies for brain shift evaluation. Medical Image Analysis. 2004; 8(4):447–464. [PubMed: 15567708]

He BJ, et al. Electrophysiological correlates of the brain's intrinsic large-scale functional architecture. Proceedings of the National Academy of Sciences of the United States of America. 2008; 105(41): 16039–16044. [PubMed: 18843113]

Hermes D, et al. Automated electrocorticographic electrode localization on individually rendered brain surfaces. Journal of Neuroscience Methods. 2010; 185(2):293–298. [PubMed: 19836416]

Hill DL, et al. Measurement of intraoperative brain surface deformation under a craniotomy. Neurosurgery. 1998; 43(3):514–526. discussion 527–528. [PubMed: 9733307]

Hill DL, et al. Sources of error in comparing functional magnetic resonance imaging and invasive electrophysiological recordings. Journal of Neurosurgery. 2000; 93(2):214–223. [PubMed: 10930006]

Hunter JD, et al. Locating chronically implanted subdural electrodes using surface reconstruction. Clinical Neurophysiology: Official Journal of the International Federation of Clinical Neurophysiology. 2005; 116(8):1984–1987. [PubMed: 16000256]

Jerbi K, et al. Task-related gamma-band dynamics from an intracerebral perspective: review and implications for surface EEG and MEG. Human Brain Mapping. 2009; 30(6):1758–1771. [PubMed: 19343801]

Kovalev D, et al. Rapid and fully automated visualization of subdural electrodes in the presurgical evaluation of epilepsy patients. AJNR American Journal of Neuroradiology. 2005; 26(5):1078–1083. [PubMed: 15891163]

Keller CJ, et al. Intrinsic functional architecture predicts electrically evoked responses in the human brain. Proc Nat Acad Sci. 2011 in press.

Leuthardt EC, et al. Electrocorticography-based brain computer interface--the Seattle experience. IEEE Transactions on Neural Systems and Rehabilitation Engineering: A Publication of the IEEE Engineering in Medicine and Biology Society. 2006; 14(2):194–198. [PubMed: 16792292]

Mahvash M, et al. Coregistration of digital photography of the human cortex and cranial magnetic resonance imaging for visualization of subdural electrodes in epilepsy surgery. Neurosurgery. 2007; 61(5 Suppl 2):340–344. discussion 344–345. [PubMed: 18091249]

Miller KJ, et al. Cortical electrode localization from X-rays and simple mapping for electrocorticographic research: The "Location on Cortex" (LOC) package for MATLAB. Journal of Neuroscience Methods. 2007; 162(1–2):303–308. [PubMed: 17343918]

Miyagi Y, Shima F, Sasaki T. Brain shift: an error factor during implantation of deep brain stimulation electrodes. Journal of Neurosurgery. 2007; 107(5):989–997. [PubMed: 17977272]

Nelles M, et al. Fusion of MRI and CT with subdural grid electrodes. Zentralblatt Für Neurochirurgie. 2004; 65(4):174–179.

Noordmans HJ, et al. Localization of implanted EEG electrodes in a virtual-reality environment. Computer Aided Surgery: Official Journal of the International Society for Computer Aided Surgery. 2001; 6(5):241–258. [PubMed: 11892001]

Penfield, W.; Jasper, HH. Epilepsy and the functional anatomy of the human brain. Little, Brown; 1954.

Ritzl EK, et al. Transforming electrocortical mapping data into standardized common space. Clinical EEG and Neuroscience: Official Journal of the EEG and Clinical Neuroscience Society (ENCS). 2007; 38(3):132–136. [PubMed: 17844941]

Sahin N, et al. Sequential processing of lexical, grammatical, and phonological information within Broca's area. Science. 2009; 326:445–449. [PubMed: 19833971]

Schaer M, et al. A surface-based approach to quantify local cortical gyrification. IEEE Transactions on Medical Imaging. 2008; 27(2):161–170. [PubMed: 18334438]

Schaer M, et al. A surface-based approach to quantify local cortical gyrification. IEEE Transactions on Medical Imaging. 2008; 27(2):161–170. [PubMed: 18334438]

Schalk G, et al. Two-dimensional movement control using electrocorticographic signals in humans. Journal of Neural Engineering. 2008; 5(1):75–84. [PubMed: 18310813]

Schalk G. Can Electrocorticography (ECoG) Support Robust and Powerful Brain-Computer Interfaces? Frontiers in Neuroengineering. 2010; 3:9. [PubMed: 20631853]

Shenoy P, et al. Generalized features for electrocorticographic BCIs. IEEE Transactions on Bio-Medical Engineering. 2008; 55(1):273–280. [PubMed: 18232371]

Talairach, J.; Tournoux, P. Co-planar stereotaxic atlas of the human brain: 3-dimensional proportional system: an approach to cerebral imaging. Thieme; 1988.

Tao JX, et al. The accuracy and reliability of 3D CT/MRI co-registration in planning epilepsy surgery. Clinical Neurophysiology: Official Journal of the International Federation of Clinical Neurophysiology. 2009; 120(4):748–753. [PubMed: 19264546]

Wellmer J, et al. Digital photography and 3D MRI-based multimodal imaging for individualized planning of resective neocortical epilepsy surgery. Epilepsia. 2002; 43(12):1543–1550. [PubMed: 12460257]

Wells WM, et al. Multimodal volume registration by maximization of mutual information. Medical Image Analysis. 1996; 1(1):35–51. [PubMed: 9873920]

Wilson JA, et al. ECoG factors underlying multimodal control of a brain-computer interface. IEEE Transactions on Neural Systems and Rehabilitation Engineering: A Publication of the IEEE Engineering in Medicine and Biology Society. 2006; 14(2):246–250. [PubMed: 16792305]

Winkler PA, et al. Usefulness of 3-D reconstructed images of the human cerebral cortex for localization of subdural electrodes in epilepsy surgery. Epilepsy Research. 2000; 41(2):169–178. [PubMed: 10940618]

Yoshor D, et al. Receptive fields in human visual cortex mapped with surface electrodes. Cerebral Cortex (New York, NY: 1991). 2007; 17(10):2293–2302.

4. Highlights

- We describe a method for localizing intracranial electrodes in individuals.
- Post-implant CT was coregistered with pre-implant MRI.
- An optimization algorithm accounted for the brain shift caused by implantation.
- Surface-based methods were used to coregister electrode arrays across patients.

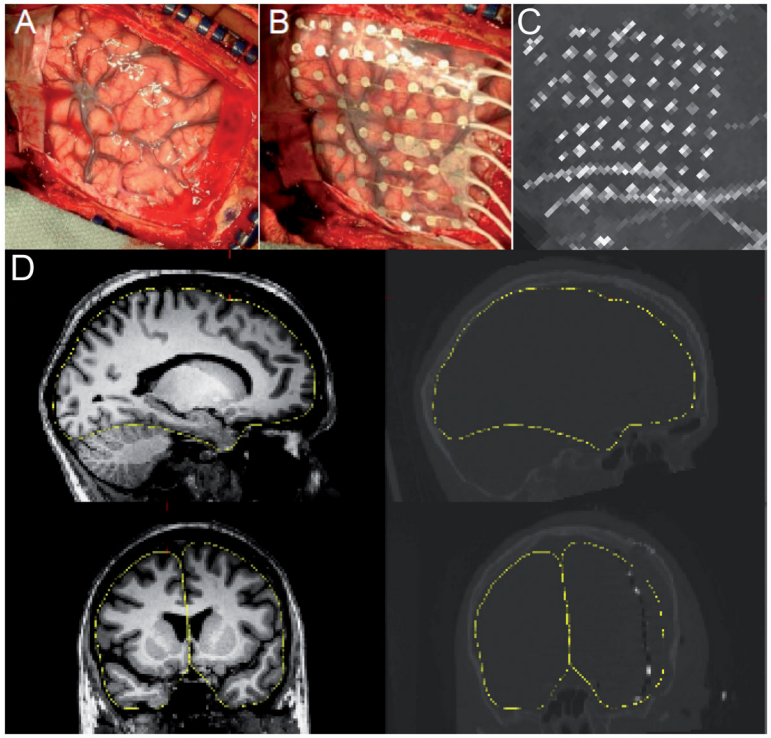

Figure 1. Intraoperative photographs, MRI-CT coregistration, and maximal-intensity projection

(**A**) Reflected dura, exposed pial surface and overlaid electrode array (**B**) from a typical craniotomy. (**C**) The sagittal maximal-intensity projection of the postoperative CT scan, showing most of the electrode sites in a single view. (**D**) Illustration of the accuracy of the coregistration between the preoperative MRI and the postoperative CT. The left panels show sagittal (top) and coronal (bottom) views of a single subject's (patient 5) MRI; the right panels show the same orientations for the postoperative CT. Electrode sites can be seen as bright spots in the coronal CT section. The yellow trace outlines the pial surface in both the MRI and CT.

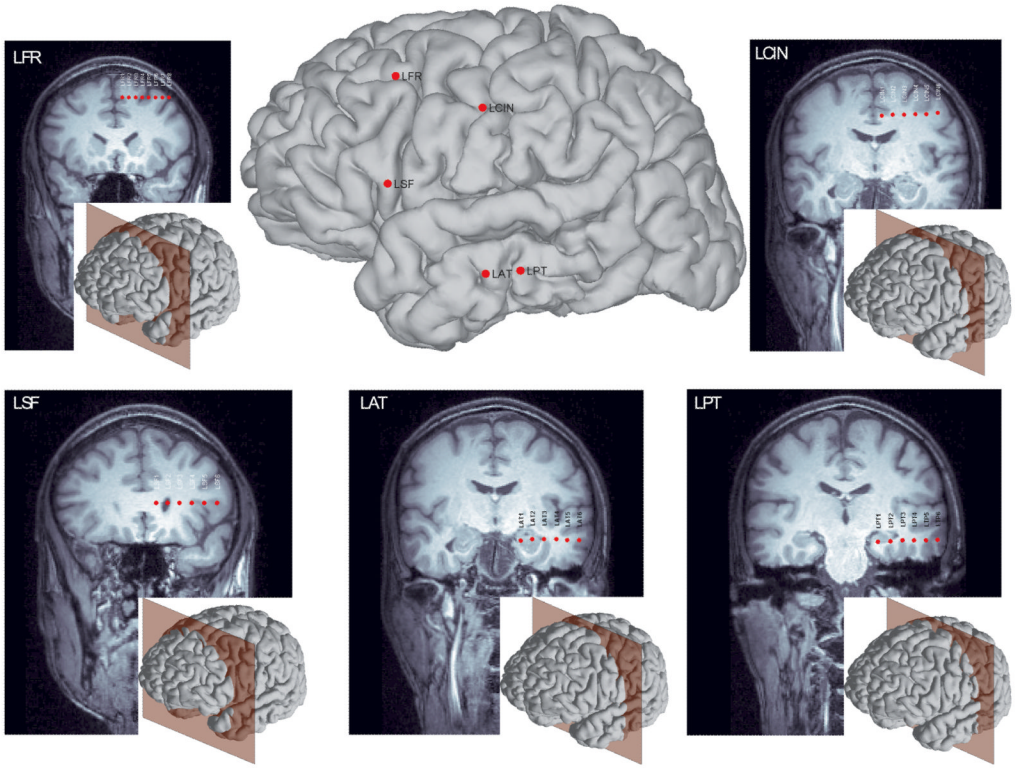

Figure 2.
Slice views of five arrays of depth electrodes after reslicing the 3D MRI volume to the long axis of each array. The middle panel shows the entry point for each array overlaid on the reconstructed cortical surface; the inset in each panel shows this patient's reconstructed cortical surface along with peri-coronally oriented planes to indicate the slice view.

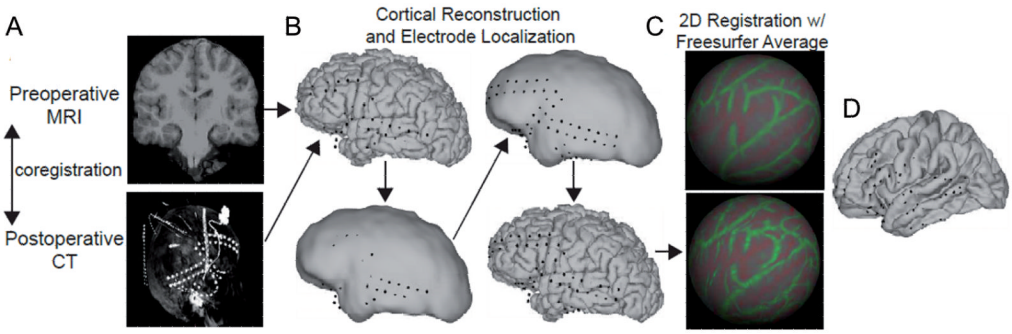

Figure 3. Outline of electrode localization and intersubject mapping procedure

(**A**) The preoperative MRI is coregistered with the postoperative CT volume. The lower panel shows the maximal intensity projection of the CT volume in the sagittal dimension, which shows all the electrodes in a sagittal plane. (**B**) Due to the parenchymal shift from the implant procedure, some electrodes initially appear as though buried in the gray matter. To correct for this, each electrode coordinate is projected first to a smoothed pial surface (effectively a dural surface) and subsequently back to the pial surface. (**C**) 2D registration with the Freesurfer average brain. An inflated spherical surface is computed from the individual's pial surface and aligned with that of the Freesurfer average. (**D**) Projection of each electrode coordinate from the individual's pial surface to that of the Freesurfer average.

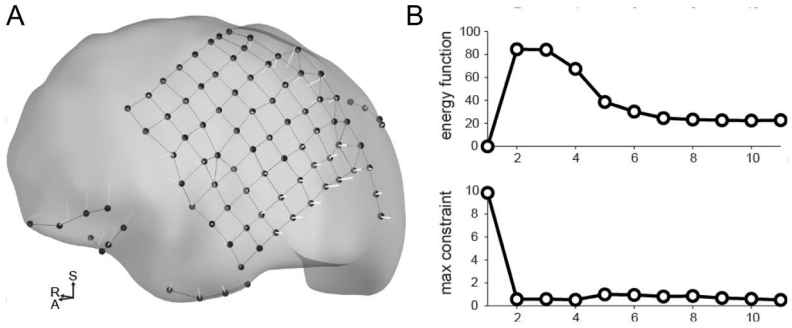

Figure 4. Illustration of the energy-minimization procedure used to project the electrode coordinates onto the cortical surface

(**A**) Dural surface showing each electrode's path from it's initial volumetric location estimate to it's final location on the dural surface. (**B**) The top panel shows the value of the energy function across successive iterations of the algorithm. Note how the function approaches a stable value as the number of iterations increases. The bottom panel shows the value of the constraint function.

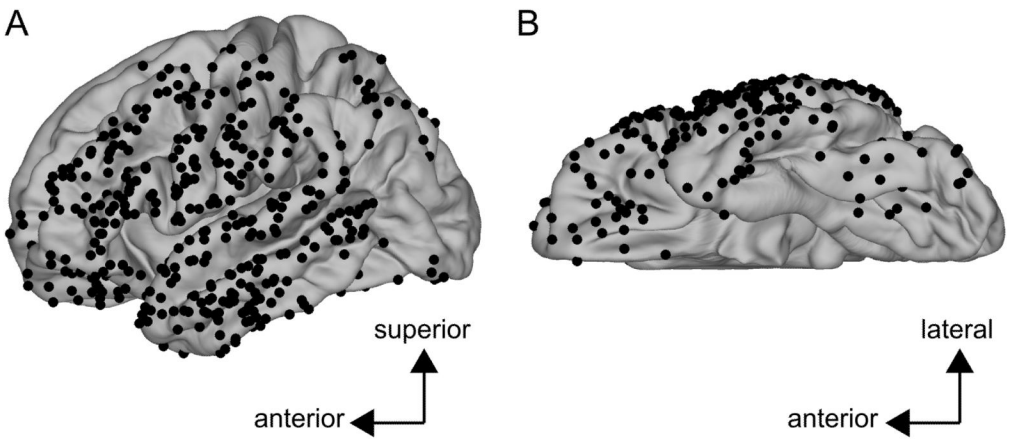

Figure 5. Electrode coordinates collapsed across all four patients mapped onto the Freesurfer average brain

Each black dot represents an electrode from one of the four patients. (**A**) Lateral view of the left hemisphere. (**B**) Inferior view of the left hemisphere.

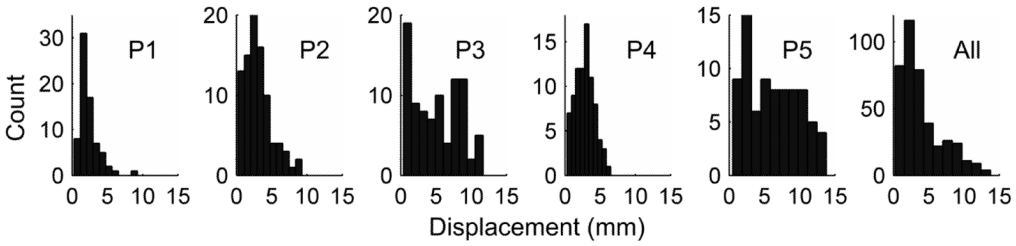

Figure 6.

Histograms of distances between initial and final (i.e. after "snapping) estimates of electrode locations yielding a measure of intracranial pressure-induced parenchyma deformation due to electrode implantation. Each of the first five panels shows the distance histograms from single patients; the right-most panel shows the distance histogram across all five patients.

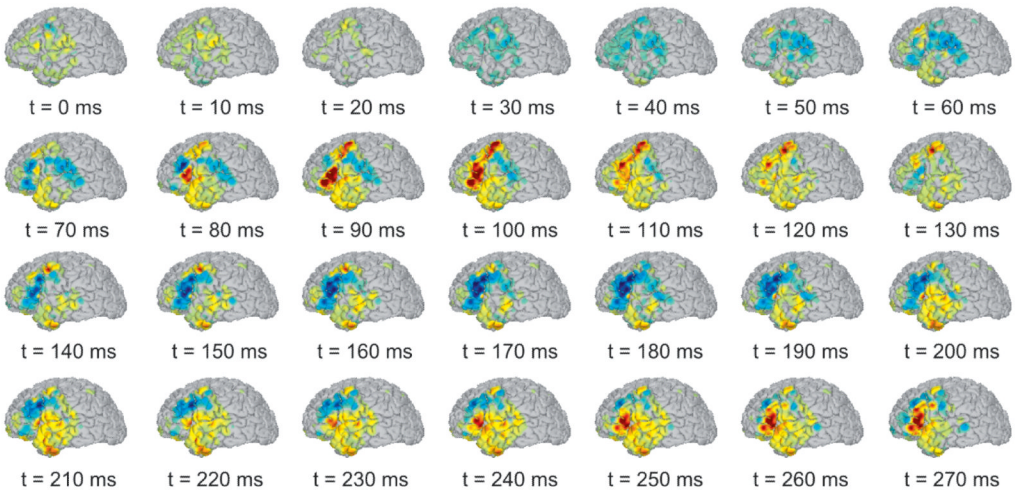

Figure 7.

Spatiotemporal voltage map of an interictal discharge from patient 5. Color intensity indicates amplitude of positive (red) or negative (blue) voltage. The discharge initiates near the border of the middle and inferior frontal gyri at approximately 70ms into the epoched time window. A post-discharge undershoot can be seen beginning around 130ms and continuing until the start of the slow wave 230ms.

Table I

Patient, implant and seizure-onset information.

Patient	Hemisphere	Sex	Age	Electrode Arrays	Seizure Focus
P1	Left	Male	21	Four 2×8 One 1×8 One 8×8	Left Anterior Temporal
P2	Left	Male	22	One 1×8 Four 1×4 One 8×8	Left Cingulate Cortex
P3	Left	Male	29	One 1×8 Four 1×4	Left Anterior Temporal and Left Parietal
P4	Left	Female	23	One 8×8 Five 1×4	Anterior Middle Frontal
P5	Left	Male	20	One 8×8 Four 1×4	Posterior Superior Temporal and Middle Frontal

Table II

Validation results. All numbers in mm.

Patient	Median	Lower Quartile	Upper Quartile	Min	Max
P3	2.52	1.27	3.66	0.05	5.56
P5	3.00	2.04	4.01	0.52	8.16